EDDY WIJANTO-FILE 8

by Eddy Wijanto-file 8 Eddy Wijanto-file 8

Submission date: 14-Feb-2023 02:13PM (UTC+0700)
Submission ID: 2013878818
File name: Optics_Communications_Journal.pdf (7.06M)
Word count: 6002
Character count: 30818

Optics Communications 486 (2021) 126778

Contents lists available at ScienceDirect

Optics Communications

journal homepage: www.elsevier.com/locate/optcom

Implementation of a fiber-based resonant beam system for multiuser optical wireless information and power transfer

Chun-Ming Huang [a], Eddy Wijanto [b], Shin-Pin Tseng [c], Yu-Hao Liu [b], Yu-Tang Luo [b], Hui-Chi Lin [b], Hsu-Chih Cheng [b,*]

[a] Department of Electronic Engineering, National Formosa University, Yunlin County 63201, Taiwan, ROC
[b] Department of Electro-Optical Engineering, National Formosa University, Yunlin County 63201, Taiwan, ROC
[c] Department of Electronic Engineering, National United University, Miaoli County 36003, Taiwan, ROC

ARTICLE INFO

Keywords:
Resonant beam
Free-space optics
Energy harvesting
Optical wireless information and power transfer

ABSTRACT

A fiber-based resonant beam system is proposed for a simultaneous optical wireless information and power transfer (OWIPT) system. A fiber Bragg grating and an optical circulator are used to achieve simultaneous wireless optical communication and power transmission. In the receiver subsystem, a communication and energy harvesting circuit is employed to separate alternating current (AC) and direct current (DC) outputs. The AC output is used for information transmission, and the DC output is used for power transfer. We conducted experiments to test the built-in safety mechanism to verify whether the resonant beam stops immediately if any obstacle obstructs the line of sight of the system. The proposed architecture can be constructed for indoor and outdoor multiuser applications. The results demonstrated that the proposed fiber-based resonant beam system can be implemented successfully for simultaneous OWIPT.

1. Introduction

Smartphones and other mobile devices have become an inseparable part of today's daily lives. Throughout the day, most people are sending messages and emails, making voice or video calls, posting on social networks, and playing online games. The increasing usage of mobile devices also increases the average daily power consumption from a typical device battery. In addition, fifth-generation (5G) mobile technologies are projected to support massive amounts of data at high bit rates with minimal delay [1]. This feature of 5G technologies will stimulate many new applications with sophisticated multimedia signal processing, which will increase battery usage.

Furthermore, rapid development of the Internet of things (IoT) is driving the demand for high-bit-rate and low-latency wireless information transfer. One challenge of the IoT is that typical IoT devices are designed to operate from battery power and have limited energy. Some IoT devices cannot have their batteries replaced. In addition, frequent battery charging for mobile devices by using conventional wired mechanisms tends to obstruct user mobility. In such cases, wireless power transmission (WPT) can be a solution. Free-space optics (FSO) is a promising WPT method [2] that provides high data rates, is immune to radio frequency (RF) interference, does not require licensing, provides a highly secure communication link, is relatively fast, and can be deployed easily. The only substantial consideration for FSO is line of sight (LOS) between the transmitter and receiver.

Simultaneous wireless information and power transfer (SWIPT) technology simultaneously transmits information signals and energy through air [3,4]. SWIPT can strike a balance between message transmission rate and energy harvesting [5]. Because of the superiority of optical systems, optical wireless power transfer (OWPT) has been investigated [6–11]. With traditional OWPT technology, it is challenging to provide watt-level power transmission across meter-level distances for IoT and mobile applications [12,13]. Distributed laser charging (DLC) may offer a wireless power solution for these problems. In DLC systems, photons are amplified regardless of their angle of incidence as long as they travel along the LOS between two retroreflectors. Hence, the intracavity laser generated by a DLC resonator can be self-aligned without the need for specific positioning or tracking. The maximum power transfer efficiency depends on the transmitter input power, laser wavelength, transmission distance, and photovoltaic (PV) cell temperature. SWIPT is possible as long as the communication and network modules are integrated into the DLC transmitter and receiver [14]. A DLC system is safe because its laser can be stopped immediately when any obstacle stands athwart the LOS. When designing any DLC system for maximal power transmission efficiency, the effects of laser wavelength, transmission attenuation, and PV cell temperature should be evaluated [15].

Light-wave power transfer can be combined with RF power transfer to utilize the bands of both transmission resources in their entirety [16].

* Corresponding author.
E-mail address: chenghc@nfu.edu.tw (H.-C. Cheng).

https://doi.org/10.1016/j.optcom.2021.126778
Received 14 July 2020; Received in revised form 25 September 2020; Accepted 7 January 2021
Available online 9 January 2021

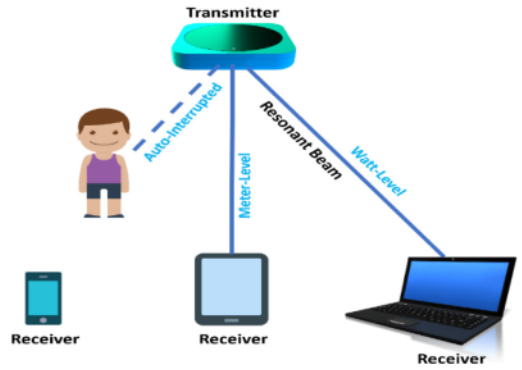

Fig. 1. Features of OWIPT.

A hybrid system can be implemented to solve the LOS consideration in light-wave power transfer and to solve the safety aspect of RF power transfer. With suitable combination protocols, a hybrid system of this type can be used to overcome the challenges of each technology and elevate the overall performance gain.

In simultaneous light-wave information and power transfer for visible light or infrared communication systems with a simple solar panel at the receiver, adjustment strategies can be deployed to balance the trade-off between the harvested energy and quality of service [17]. Such strategies include making separate adjustments to transmission and reception and coordinated adjustments to transmission and reception. With careful adjustments, the maximum harvested energy, information rate, and signal-to-noise plus interference ratio can be optimized.

Various optical wireless information and power transmission (OWIPT) systems based on resonant light have been demonstrated in several experiments [5,18,19]. In this type of system, a gain medium is placed between the transmitting and receiving ends of the module. Light bounces off the mirror; as the light oscillates back and forth, the system develops resonant light. A resonant beam charging (RBC) system can transmit wireless power from a transmitter to a receiver through a resonant beam. A typical RBC system includes a current regulator, diode pump, gain medium, two retroreflectors—R_1 and R_2, and a PV panel [5]. Fig. 1 illustrates the features of an OWIPT system based on a resonant beam. In a typical WPT or wireless information transmission (WIT) system that utilizes a laser as a source, a high-intensity laser beam must be emitted from a specific distance to the receiver end. A laser-based WPT or WIT usually faces the challenges of mobility and safety; therefore, they typically are used only for low-power and short-distance applications [5]. To overcome the limitations of typical laser-based WPT or WIT systems, the OWIPT system in this study enabled high-power beam transmission through a laser resonant cavity. This RBC-based OWIPT system utilized a resonant beam to transmit watt-level power over meter-level ranges and to multiple mobile devices concurrently. In the case that any obstacle blocks the beam, the resonant beam path stops the resonance mechanism immediately. When any obstacle is in the transmission path, diffraction loss in the cavity increases. Then, if the diffraction loss becomes larger than the system gain produced by the gain medium, the resonance terminates instantly. Conversely, when the obstacle moves out of the transmission path, the loss becomes smaller than the gain factor; therefore, the resonance is immediately reconstituted.

Another method to realize a resonant beam mechanism was developed using diverging angular dispersion and spatially distributed

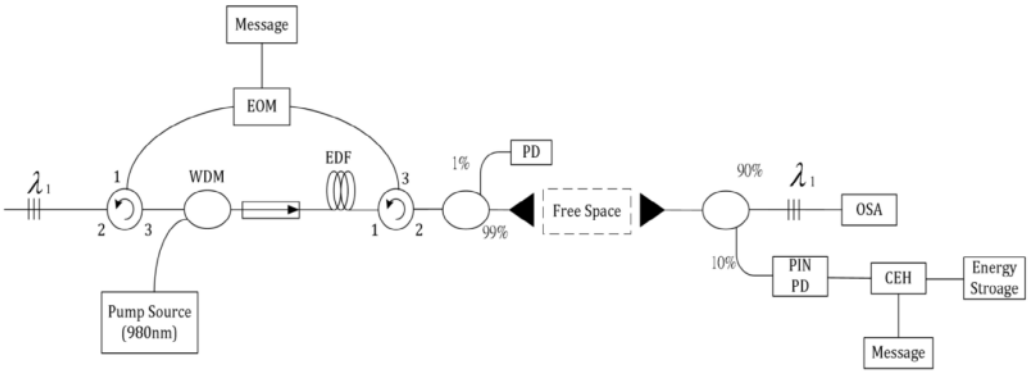

Fig. 2. Fiber-based OWIPT architecture.

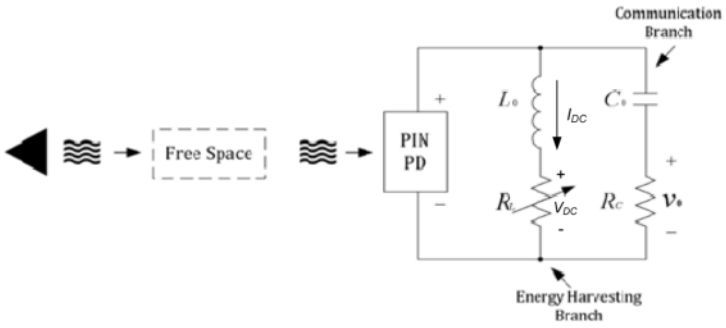

Fig. 3. CEH equivalent circuit.

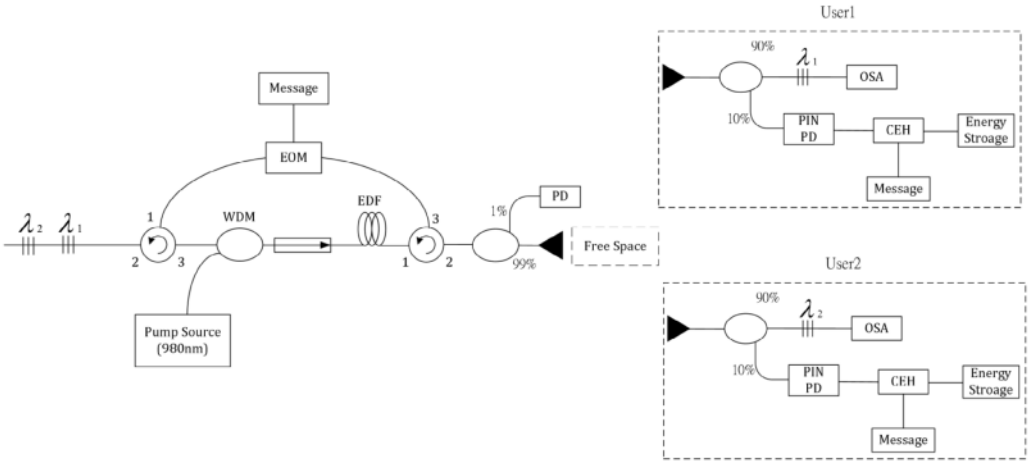

Fig. 4. Multiuser fiber-based OWIPT architecture.

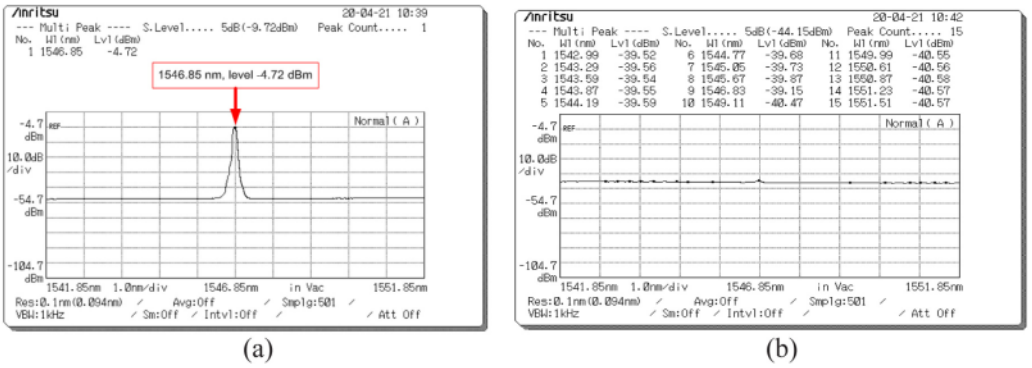

Fig. 5. Spectrum of λ_1 at the first detection point in the (a) uninterrupted scenario and (b) interrupted scenario.

laser cavity resonance [18]. A diffraction grating was used to disperse broadband light, and the field of view was expanded using a telescope. To realize the self-alignment feature, retroreflectors reflected the incident beam to complete the resonant beam mechanism. As a built-in safety mechanism, when any vulnerable organ obstructs the LOS of this OWIPT system, the resonance beam is stopped.

The design of the OWIPT receiver plays a crucial role in increasing the efficiency of the system in terms of receiving power. An optical wireless communication receiver that uses a solar panel as a photodetector was proposed in [19]. This system supported simultaneous data transmission and power transfer. Solar panels were used to convert modulated optical signals into electrical signals without the use of any external power. Energy was harvested from the direct current (DC) output of the modulated light; the information signal was obtained from the alternating current (AC) output by using orthogonal frequency-division multiplexing as the signature code.

In the present study, we developed a fiber-based resonant beam system for OWIPT. The resonant beam effect was produced by using all-fiber components. We conducted experiments in both uninterrupted and interrupted scenarios. The interrupted scenario demonstrated the safety mechanism of the proposed system. The all-fiber system is beneficial for far-field OWIPT applications because it is free of electromagnetic interference and does not affect existing radio communications. The system architecture and implementation of the proposed fiber-based resonant beam system for single and multiple users are explained in this paper.

The remainder of this paper is organized as follows. Section 2 introduces the proposed fiber-based OWIPT system, including the system architecture, the derivation of optical power transmission, and the multiuser scheme. Section 3 presents the experimental results for single-user and multiuser fiber-based OWIPT systems in both uninterrupted and interrupted scenarios. Finally, our conclusions are presented in Section 4.

2. Proposed fiber-based OWIPT system

The working principle of the proposed fiber-based OWIPT system is based on the RBC system. Two fiber Bragg gratings (FBGs) of the same central wavelength (λ_1) are used to generate resonant light for the RBC. In the transmitter subsystem, an erbium-doped fiber amplifier (EDFA) that provides a stable 980-nm laser is used as the pumped source for wavelength division multiplexing (WDM). After the optical signals from the EDFA-pumped laser source pass through the WDM and isolator, they are received by an erbium-doped fiber (EDF) that amplifies and converts the signals into the 1550-nm band. The isolator is used to prevent the incidence of unwanted feedback light. From the EDF, the optical signals then pass through the optical circulator, which separates the optical signals traveling in opposite directions. An optical coupler is used to split these optical signals into two output sources, 1% for optical power monitoring and 99% for transmission into free space. The specified wavelength from FBG is then reflected back to the circulator to complete the resonance effect. For information

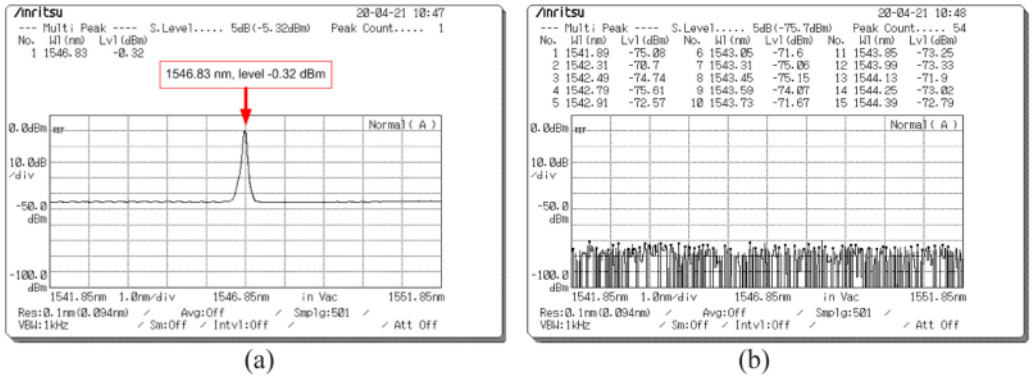

Fig. 6. Spectrum of λ_1 at the second detection point in the (a) uninterrupted scenario and (b) interrupted scenario.

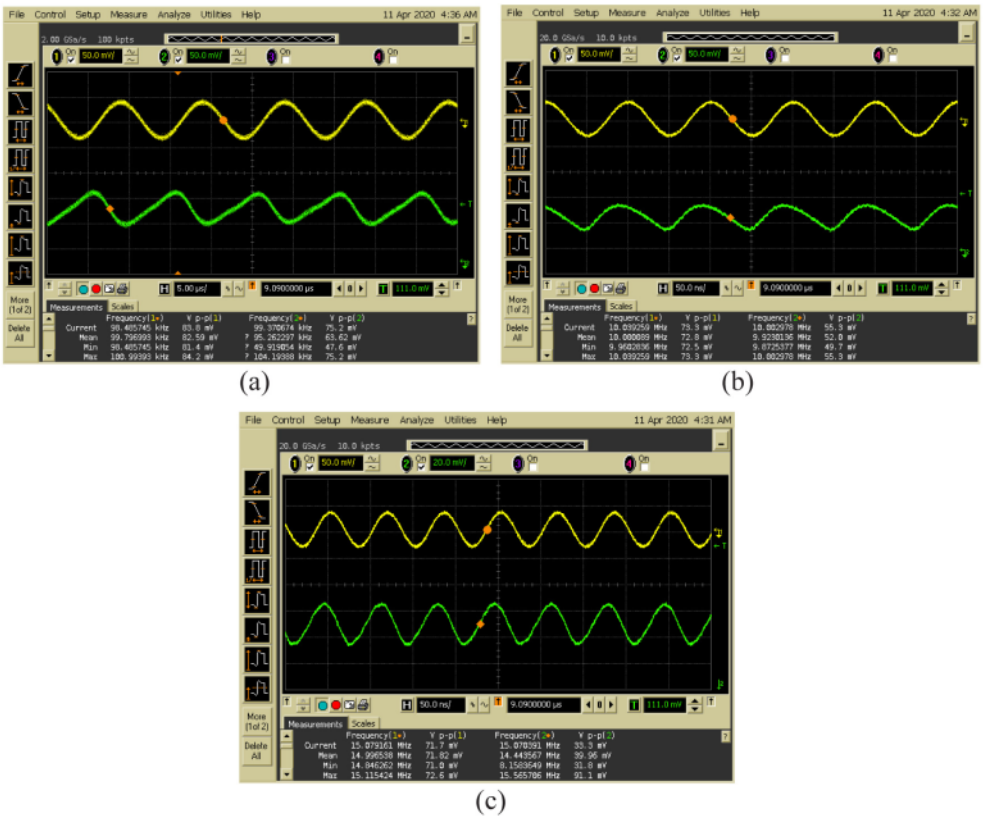

Fig. 7. Waveform of λ_1 at the first detection point for the signal frequencies of (a) 100 kHz, (b) 10 MHz, and (c) 15 MHz.

transmission, an electro-optical modulator (EOM) is used to modulate the optical signals. The construction of the proposed fiber-based OWIPT is detailed in Fig. 2.

In the receiver subsystem, the photodetector (PD) receives light and converts it into electrical signals. The AC and DC elements of the received signal are separated using a communication and energy harvesting (CEH) circuit to complete the process of DC power storage and AC signal transmission. Power storage is expressed in terms of DC current (I_{DC}) and DC voltage (V_{DC}) measured at the DC part. The CEH equivalent circuit is illustrated in Fig. 3. In the experiment, $L_0 = 50$ mH, $C_0 = 330$ μF, $R_L = 0.6$ Ω, and $R_C = 470$ Ω were used.

Optical power transmission based on fiber-optic resonant beam transmission technology can be divided into three stages, namely pumping laser power (P_{pump}) formed by input current, receiving laser output power (P_{laser}), and PD output power after photoelectric conversion ($P_{pv,o}$). The function of P_{pump} as input current I_{in} can be expressed as follows [5]:

$$P_{pump}\left(I_{in}\right) = \frac{hC}{q\lambda}\eta_e\left[I_{in} - I_{th}\right] \tag{1}$$

where h is Planck's constant, C is the speed of light in vacuum, q is the electron charge, λ is the operating wavelength, η_e is the external

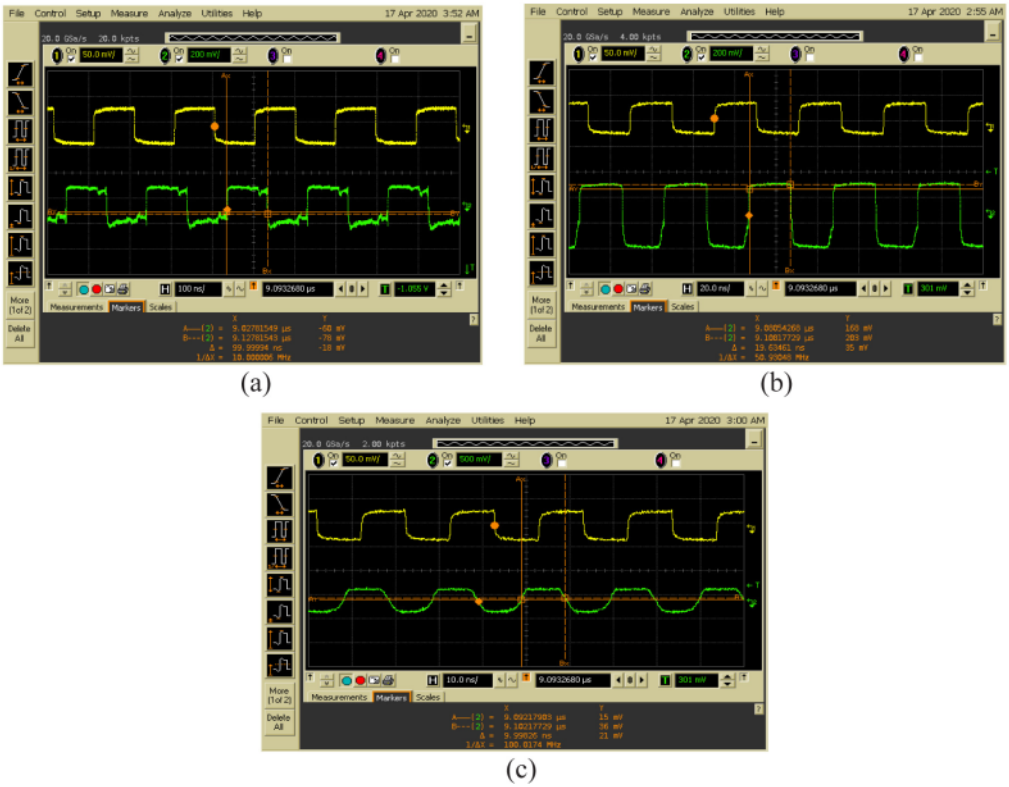

Fig. 8. Waveform of λ_1 at the first detection point under the bit rates of (a) 10 Mbps, (b) 50 Mbps, and (c) 100 Mbps.

quantum efficiency, and I_{th} is the critical current. The laser output power P_{laser} at the receiving end can be computed as follows [5]:

$$P_{laser} = \eta_{store} P_{pump} f(d) + C \tag{2}$$

where η_{store} is the conversion efficiency of population reversal, $f(d)$ is a function of the internal parameters, where d is the distance between two terminals, and C is a constant value depending on the internal parameters.

The current–voltage (I–V) characteristics of the PD can be computed as follows [5]:

$$I_{pv,o} = I_{ph} - I_d - \frac{V_d}{R_{sh}} \tag{3}$$

$$I_d = I_0 \left(e^{\frac{V_d}{n_s n V_T}} - 1 \right) \tag{4}$$

$$V_d = V_{pv,o} + I_{pv,o} R_s \tag{5}$$

where I_0 is the reverse saturation current, n_s is the number of PDs in series, n is the diode ideal factor, $V_T = \frac{kT}{q}$ is the junction thermal voltage of the diode, k is the Boltzmann constant, and T is the temperature (K). Given the input optical power $P_{pv,i}$ of the PD, the photogenerated current I_{ph} can be written as follows [5]:

$$I_{ph} = \rho P_{pv,i} \tag{6}$$

where ρ is the responsivity (A/W) of the photoelectric conversion. Eq. (6) can be used to prove the linear relationship between the photogenerated current (I_{ph}) and the input optical power ($P_{pv,i}$).

If the temperature changes slowly, η_e can be assumed to be constant, and the distance d in $f(d)$ can be assumed to be constant attenuation, η_d, at a certain distance. The output current of the PD can be operated in a linear range according to the following formula [5]:

$$I_{pv,o} \approx I_{ph} = \rho \left\{ \eta_{store} \eta_d \left\{ \frac{hC}{q\lambda} \eta_e \left[I_{in} - I_{th} \right] \right\} + C \right\}$$
$$= \gamma \left[I_{in} - I_{th} \right] + \beta \tag{7}$$

$$\gamma = \rho \eta_{store} \eta_d \eta_e \frac{hC}{q\lambda} \tag{8}$$

$$\beta = \rho C \tag{9}$$

where both γ and β are constants. This demonstrates the linear modulation of wireless optical information systems based on resonant beams.

Expanded experiments can involve multiuser OWIPT schemes, which can allow users in different bands to use fiber-based RBC architectures. Fig. 4 illustrates an architecture for two users. For more than two users, this architecture can be expanded by following the same principle.

In the transmitter, two FBGs (λ_1 and λ_2) reflect different users' optical signals. Because the transmitter is paired with one or more receivers, each user utilizes one pair of FBGs with the same wavelength for resonating. In the experiment, two pairs of FBGs with different wavelengths (λ_1 and λ_2) were used for user #1 and user #2, respectively. In the receiver, an FBG of the corresponding wavelength is used to split the signals across users. The optical signals are divided into two branches. The first branch is used to reflect the signals back into the circulator, thus completing the resonant beam scheme. The second branch is used for information and power harvesting. The reflected optical signal enters the EOM and is modulated using a signal generator for information transmission. In this experiment, the information sent from the message part to the EOM is a broadcast message from one transmitter to two receivers.

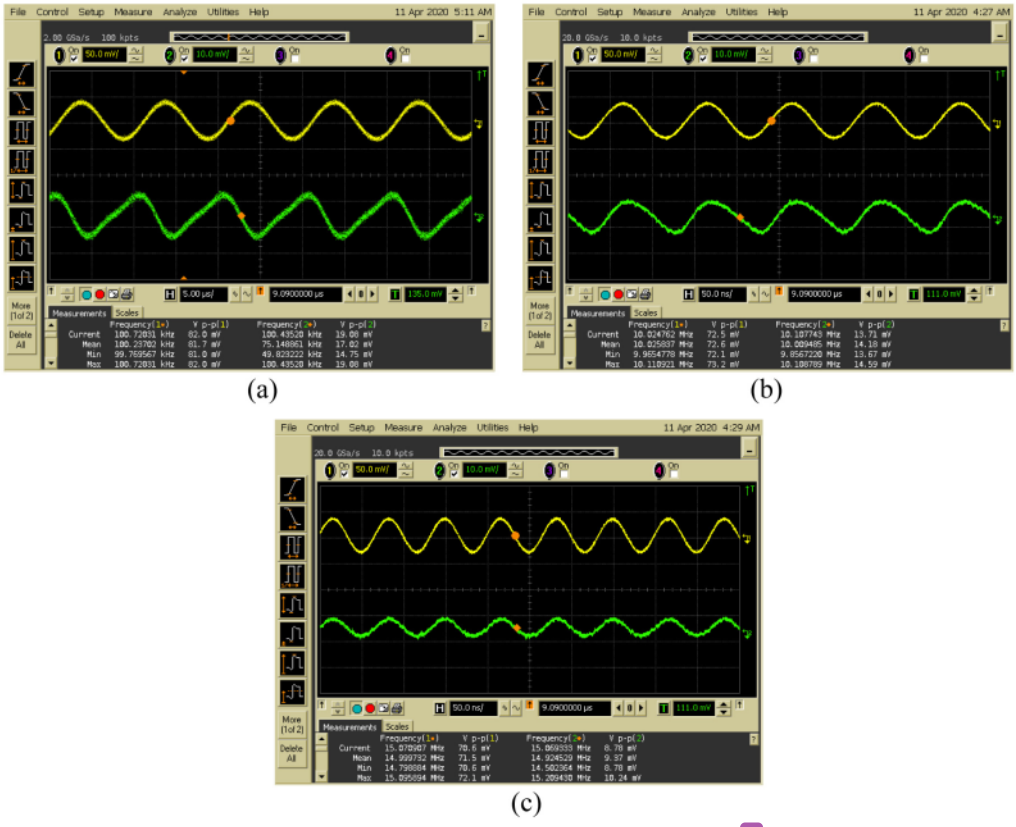

Fig. 9. Waveform of λ_1 originating from *Rc* in the CEH circuit under the signal frequencies of (a) 100 kHz, (b) 10 MHz, and (c) 15 MHz.

3. Experimental results

The purpose of the first experiment was to verify the feasibility of the proposed fiber-based resonant beam OWIPT. To this end, we first conducted an experiment to determine whether the OWIPT system signal had the desired resonance effect. In this experiment, EDFA was used to provide a stable 980-nm pumped laser source. The EDF received the EDFA-pumped laser source signal and converted it into a 1550-nm band source signal. Uniform FBGs (Reflectivity 99%, 3L Technologies Inc., Taiwan) with central wavelengths of 1546 nm (λ1) and 1549 nm (λ_2) were used to realize the resonance effect. A collimator was used to align the light such that it was transmitted as a parallel light output. Optical couplers (Fiber Optic Communications, Inc., Taiwan) were used as 1 × 2 splitters, and a 10-Gb/s integrated optic intensity modulator (Pirelli, Italy) was used to modulate the signal of the pattern output. A 33120A pulse pattern generator (Hewlett Packard, United States) was used to generate the desired patterns for information transmission. A single-mode circulator (1550 nm and 500 mW; FCIR-1550-3-3-A-0-1-2-1-2) was used as the optical circulator, and a PD with ±15 V constant voltage–current limiting power supply (model-1601, New Focus, California) was used to convert the optical signals into electrical signals. A 2-mm InGaAs PIN photodetector (PIN PD) was used to receive and forward the electrical signal into the CEH circuit. An oscilloscope (OSC, TDS2102B, Tektronix, Oregon, United States) was used to monitor the PD outputs, and an optical spectrum analyzer (MS9710C, Anritsu, Japan) was employed to assess the accuracy of the spectral output. The range of free space in this experiment was 10 cm. The component specifications of the CEH circuit are summarized in Table 1.

The output of the optical coupler was the first detection point at the transmission end, and it was used for optical power monitoring.

Table 1
Component specifications of the CEH circuit.

Component	L_0	C_0	R_L	R_C
Specification	50 mH	330 μF	0.6 Ω	470 Ω

The second detection point was the transmission end of the FBG, and it was used to detect whether a resonant beam had been produced.

First, we conducted experiments for the single-user scheme. Fig. 5 depicts the spectrum of λ_1 recorded at the first detection point. Fig. 5(a) illustrates the spectrum of λ_1 without interruption, where the light intensity is approximately −4.72 dBm while Fig. 5(b) shows the spectrum after interruption. This figure indicates no resonance effect at this time. No significant spectrum was detected; only a noise-level spectrum was produced from the reflection wavelength of the FBG at the transmission end.

Fig. 6 shows the spectrum of λ_1 recorded at the second detection point. Fig. 6(a) depicts the spectrum without interruption, where the light intensity is −0.32 dBm. After the light passes through free space, the light's power is attenuated. Furthermore, Fig. 6(b) depicts the spectrum after interruption when only a noise-level signal was left, indicating that the signal and the resonant light had not been received. These results prove that the system is safe for users because in the presence of an obstacle, no power is received.

To verify the resonance effect in the fiber loop, the signals from the detection point were observed at several EOM frequencies. Fig. 7 presents the waveform of λ_1 at the first detection point for various frequencies. First of all, Fig. 7(a) illustrates the waveform for the EOM frequency of 100 kHz. The resonant waveform (CH#1) and the

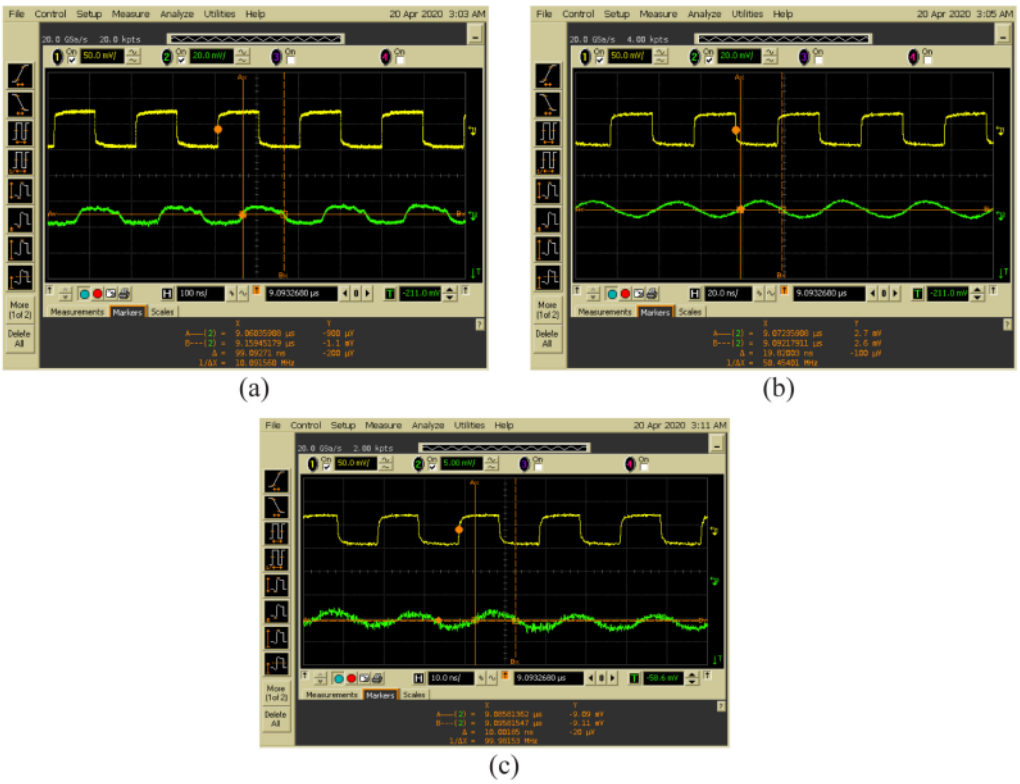

Fig. 10. Waveform of λ_1 originating from *Rc* in the CEH circuit under the bit rates of (a) 10 Mbps, (b) 50 Mbps, and (c) 100 Mbps.

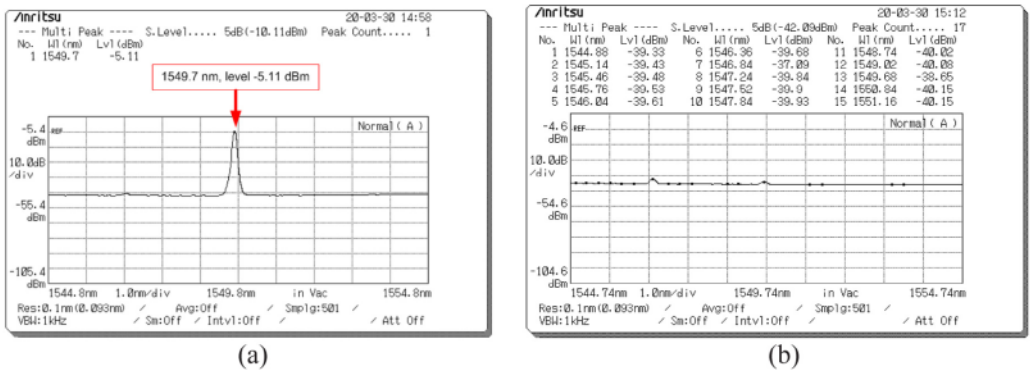

Fig. 11. Spectrum of λ_2 at the first detection point for (a) uninterrupted scenario and (b) interrupted scenario.

reference waveform (CH#2) have the same frequencies, indicating that the EOM successfully modulated the optical signals in the fiber loop. The peak-to-peak voltages of the resonant waveform and reference waveform are 83.8 and 75.2 mV, respectively. Subsequently, Fig. 7(b) shows the waveform for the EOM frequency of 10 MHz. The same frequency is produced by CH#1 and CH#2, thus proving that the optical signals are successfully modulated by EOM in the fiber loop. The peak-to-peak voltage of the resonant waveform and reference waveform are 73.3 and 55.3 mV, respectively. Afterwards, Fig. 7(c) demonstrates the waveform corresponding to the EOM frequency of 15 MHz. The frequencies measured at CH#1 and CH#2 are identical, indicating that the EOM completely modulated the optical signals in the fiber loop. The peak-to-peak voltages of the resonant waveform and reference waveform are 71.7 and 33.3 mV, respectively.

Because bit rate affects system performance, we observed the waveforms at the detection points under different bit rates. Fig. 8 illustrates the waveform of λ_1 at the first detection point under different bit rates.

Firstly, Fig. 8(a) displays the waveform under the bit rate of 10 Mbps. CH#1 and CH#2 have the same frequency, indicating successful modulation of the optical signals by the EOM in the fiber loop. The voltage difference is −18 mV. Next, Fig. 8(b) graphs the waveform corresponding to the bit rate of 50 Mbps. CH#1 and CH#2 have the same frequency, which indicates that the EOM successfully modulated the optical signals in the fiber loop. The voltage difference is 35 mV.

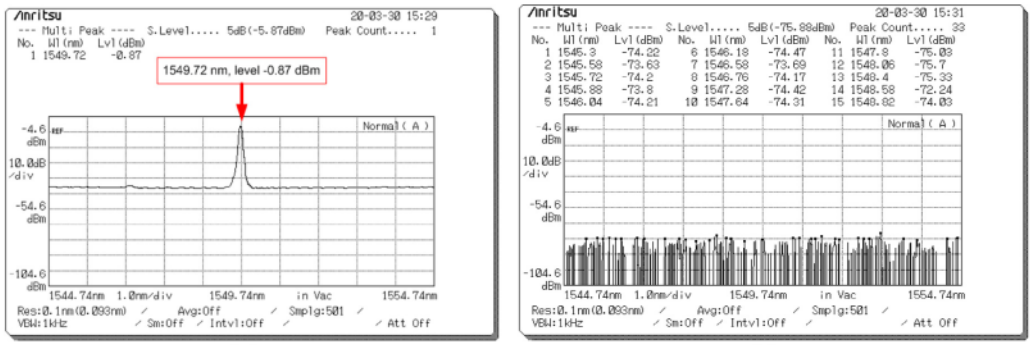

Fig. 12. Spectrum of λ_2 at the second detection point for (a) uninterrupted scenario and (b) interrupted scenario.

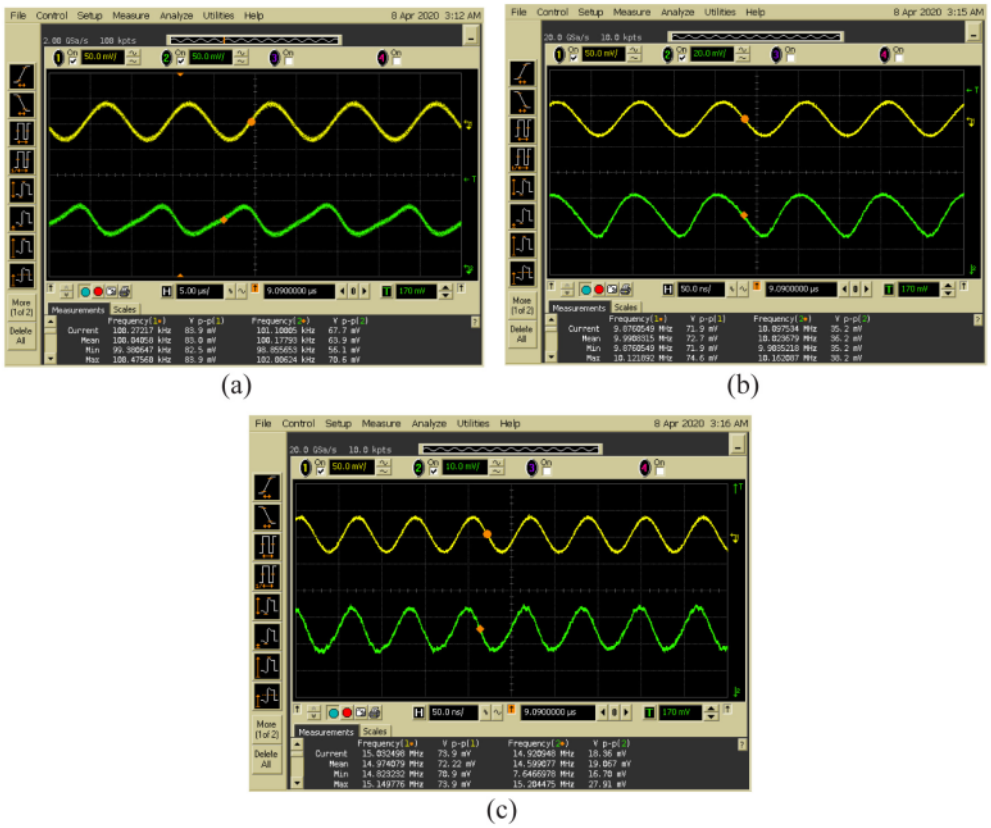

Fig. 13. Waveform of λ_2 at the first detection point under the signal frequencies of (a) 100 kHz, (b) 10 MHz, and (c) 15 MHz.

After that, Fig. 8(c) illustrates the waveform under the bit rate of 100 Mbps. CH#1 and CH#2 have the same frequency, thus indicating that the EOM successfully modulated the optical signals in the fiber loop. The voltage difference is 21 mV.

Next, the waveforms of the CEH subsystem were observed to monitor the performance of the proposed system. Fig. 9 shows the waveform of λ_1 originating from the *Rc* in the CEH circuit.

Initially, Fig. 9(a) shows the waveform obtained with the EOM frequency of 100 kHz. CH#1 and CH#2 have the same frequency, thus indicating complete modulation of the optical signals by the EOM in the fiber loop. The peak-to-peak voltages of the resonant waveform and reference waveform are 82 and 19.08 mV, respectively. Further, Fig. 9(b) plots the waveform obtained with the EOM frequency of 10 MHz. CH#1 and CH#2 have the same frequency, thus indicating successful modulation of the optical signals in the fiber loop by the EOM. The peak-to-peak voltages of the resonant waveform and reference waveform are 72.5 and 13.71 mV, respectively. Lattermost, Fig. 9(c) displays the waveform obtained with the EOM frequency of 15 MHz. CH#1 and CH#2 have the same frequency, thus verifying successful modulation of the optical signals. The peak-to-peak voltages of the

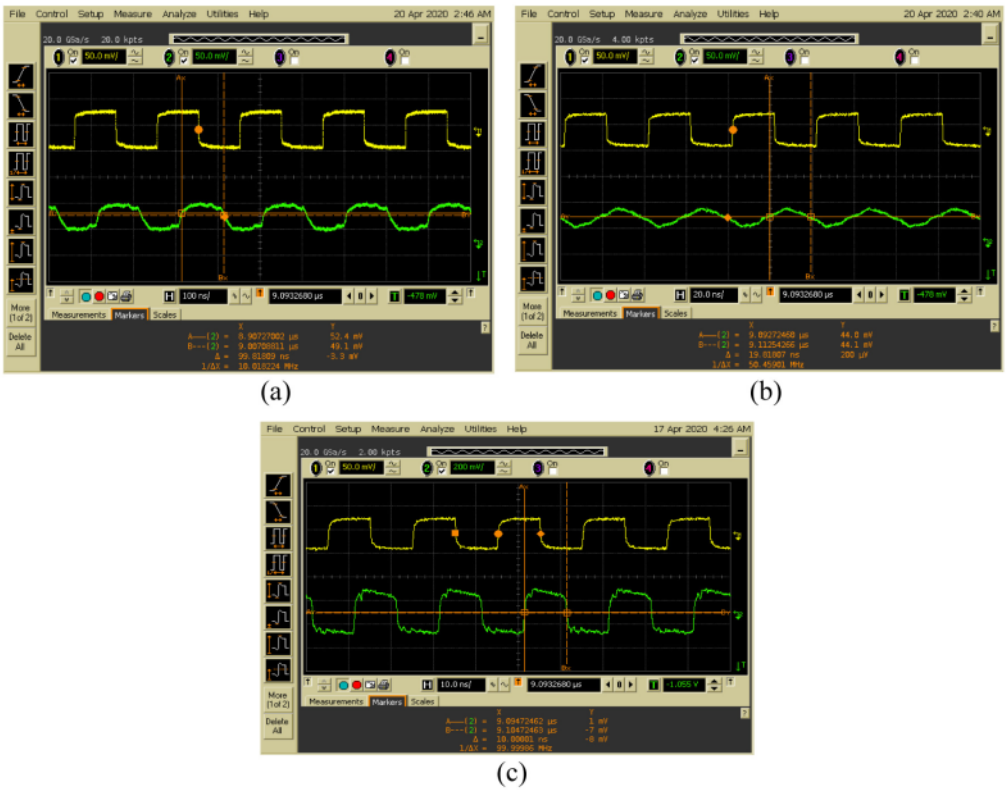

Fig. 14. Waveform of λ_2 at the first detection point under the bit rates of (a) 10 Mbps, (b) 50 Mbps, and (c) 100 Mbps.

Table 2
CEH parameters under different signal frequencies for λ_1.

CEH parameters	Frequency		
	100 kHz	10 MHz	15 MHz
DC current	0.99 mA	0.98 mA	0.98 mA
DC voltage	0.60 mV	0.59 mV	0.59 mV
AC voltage	82.00 mV_{pp}	72.50 mV_{pp}	70.60 mV_{pp}

Table 3
CEH parameters under different bit rates for λ_1.

CEH parameters	Bit rate		
	10 Mbps	50 Mbps	100 Mbps
DC current	1.05 mA	1.03 mA	1.03 mA
DC voltage	0.63 mV	0.62 mV	0.62 mV

resonant waveform and reference waveform are 70.6 and 8.78 mV, respectively.

The waveforms originating from the CEH subsystem under different bit rates were measured for the single-user scheme. Fig. 10 presents the waveform of λ_1 originating from *Rc* in the CEH circuit under different bit rates. Fig. 10(a) presents the waveform under the bit rate of 10 Mbps. CH#1 and CH#2 have the same frequency, indicating complete modulation of optical signals in the fiber loop. The voltage difference is −200 μV. Then, Fig. 10(b) demonstrates the waveform under bit rate of 50 Mbps. CH#1 and CH#2 have the same frequency, thus proving modulation of optical signals in the fiber loop. The voltage difference is −100 μV. Afterwards, Fig. 10(c) depicts the waveform under the bit rate of 100 Mbps. CH#1 and CH#2 have the same frequency, verifying full modulation of optical signals in the fiber loop. The voltage difference is −20 μV.

Tables 2 and 3 summarize the resulting CEH parameters for various frequencies and bit rates, respectively. The DC current and voltage were relatively stable across all frequencies and bit rates.

We conducted a second experiment for the multiuser scheme. When the collimator at the transmitter and the collimator at receiver #2 were aligned, the wavelength of the resonant beam changed from 1546.83 nm (λ_1) to 1549.7 nm (λ_2). Furthermore, the message modulated at the central wavelength of λ_2 from the transmitter could be reconstructed by the FBG of receiver #2 operating at the corresponding wavelength of λ_2.

Fig. 11 shows the spectrum of λ_2 recorded at the first detection point. First, Fig. 11(a) illustrates the spectrum recorded in the scenario without any interruption. The light intensity is approximately −5.11 dBm. In the other hand, Fig. 11(b) shows the spectrum recorded after an interruption. No resonance effect exists at this time, and only a small spectrum is produced owing to the reflection wavelength of the FBG at the transmitting end.

Fig. 12 demonstrates the spectrum of λ_2 at the second detection point. Initially, Fig. 12(a) depicts the spectrum without interruption. The light intensity is −0.87 dBm. The light power is attenuated after passage through free space. Conversely, Fig. 12(b) shows the spectrum after interruption, in which only noise remains. These results demonstrate the effectiveness of the safety mechanism for users in the presence of obstacles along the LOS.

Fig. 13 presents the waveforms recorded at the first detection point under different frequencies. First of all, Fig. 13(a) illustrates the waveform corresponding to the EOM frequency of 100 kHz. CH#1 and CH#2 have the same frequency, thus verifying complete modulation

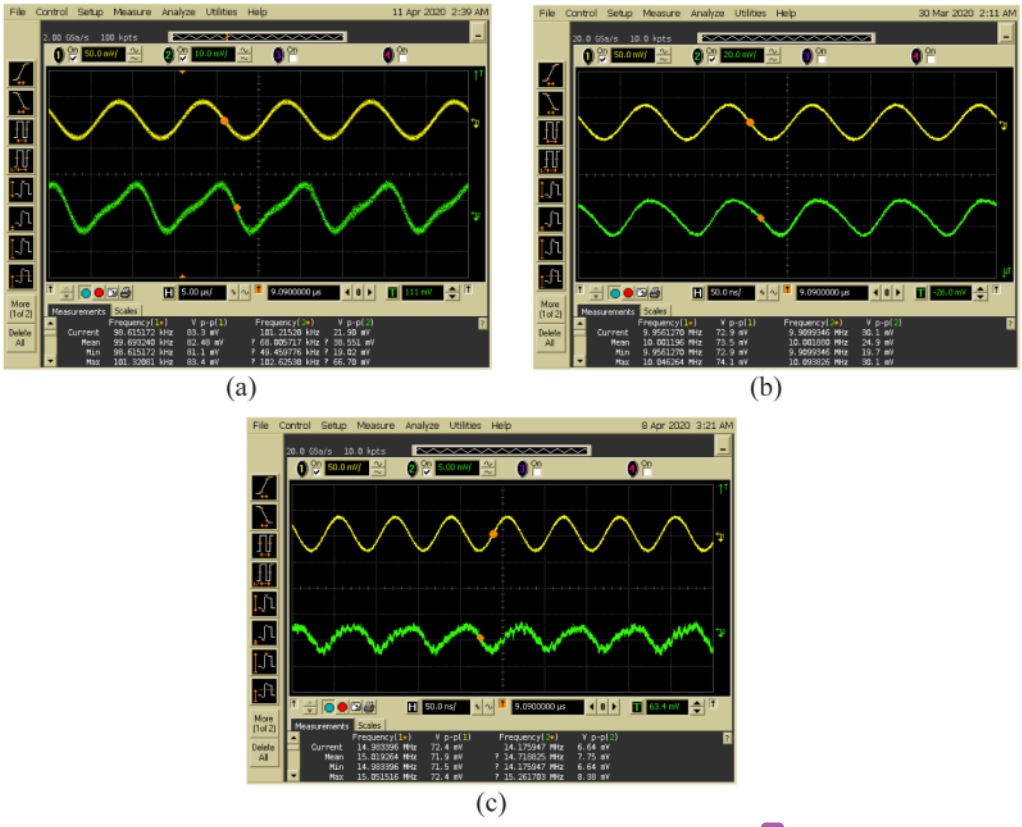

Fig. 15. Waveform of λ_2 originating from the *Rc* in the CEH circuit under the signal frequencies of (a) 100 kHz, (b) 10 MHz, and (c) 15 MHz.

of the optical signals in the fiber loop. The peak-to-peak voltages of the resonant waveform and reference waveform are 83.9 and 67.7 mV, respectively. Further, Fig. 13(b) shows the waveform corresponding to the EOM frequency of 10 MHz. CH#1 and CH#2 have the same frequency, thus indicating full modulation by the EOM in the fiber loop. The peak-to-peak voltages of the resonant waveform and reference waveform are 71.9 and 35.2 mV, respectively. Subsequently, Fig. 13(c) demonstrates the waveform corresponding to the EOM frequency of 15 MHz. CH#1 and CH#2 have the same frequency, thus indicating successful modulation of the optical signals in the fiber loop. The peak-to-peak voltages of the resonant waveform and reference waveform are 73.9 and 18.36 mV, respectively.

In a manner similar to that used for the single-user scheme, we tested system performance under different bit rates. Fig. 14 shows the waveform of λ_2 at the first detection point under different bit rates. Initially, Fig. 14(a) shows the waveform under the bit rate of 10 Mbps. CH#1 and CH#2 have the same frequency, thus verifying complete modulation of the optical signals in the fiber loop. The voltage difference is −3.3 mV. Later, Fig. 14(b) shows the waveform under the bit rate of 50 Mbps. CH#1 and CH#2 have the same frequency, thus proving modulation by the EOM in the fiber loop. The voltage difference is 200 μV. At last, Fig. 14(c) illustrates the waveform under the bit rate of 100 Mbps. CH#1 and CH#2 have the same frequency, thus verifying successful modulation of the optical signals in the fiber loop. The voltage difference is −8 mV.

The next experiment involved measurement of the CEH circuit. Fig. 15 reveals the waveform of λ_2 originating from the *Rc* in the CEH circuit. First, Fig. 15(a) shows the waveform corresponding to the EOM frequency of 100 kHz. CH#1 and CH#2 have the same frequency, thus indicating full modulation in the fiber loop. The peak-to-peak voltages of the resonant waveform and reference waveform are 83.3 and 21.9 mV, respectively. Subsequently, Fig. 15(b) exhibits the waveform corresponding to the EOM frequency of 10 MHz. CH#1 and CH#2 have the same frequency, thus verifying complete modulation of the optical signals in the fiber loop. The peak-to-peak voltages of the resonant waveform and reference waveform are 72.9 and 30.1 mV, respectively. Finally, Fig. 15(c) displays the waveform corresponding to the EOM frequency of 15 MHz. CH#1 and CH#2 have the same frequency, thus verifying modulation by the EOM in the fiber loop. The peak-to-peak voltages of the resonant waveform and reference waveform are 72.4 and 6.64 mV, respectively.

Fig. 16 presents the waveform of λ_2 originating from the *Rc* in the CEH circuit under different bit rates. First of all, Fig. 16(a) illustrates the waveform corresponding to the bit rate of 10 Mbps. CH#1 and CH#2 have the same frequency, thus verifying successful EOM modulation of the optical signals in the fiber loop. The voltage difference is 690 μV. Afterwards, Fig. 16(b) demonstrates the waveforms corresponding to the bit rate of 50 Mbps. CH#1 and CH#2 have the same frequency, thus indicating complete modulation of the optical signals by the EOM in the fiber loop. The voltage difference is 350 μV. Lattermost, Fig. 16(c) shows the waveform corresponding to the bit rate of 100 Mbps. CH#1 and CH#2 have the same frequency, thus indicating full modulation of the optical signals in the fiber loop. The voltage difference is −200 μV.

Tables 4 and 5 summarize the CEH parameters for various frequencies and bit rates, respectively. The DC currents and voltage generated by the proposed system were relatively stable across all frequencies and bit rates.

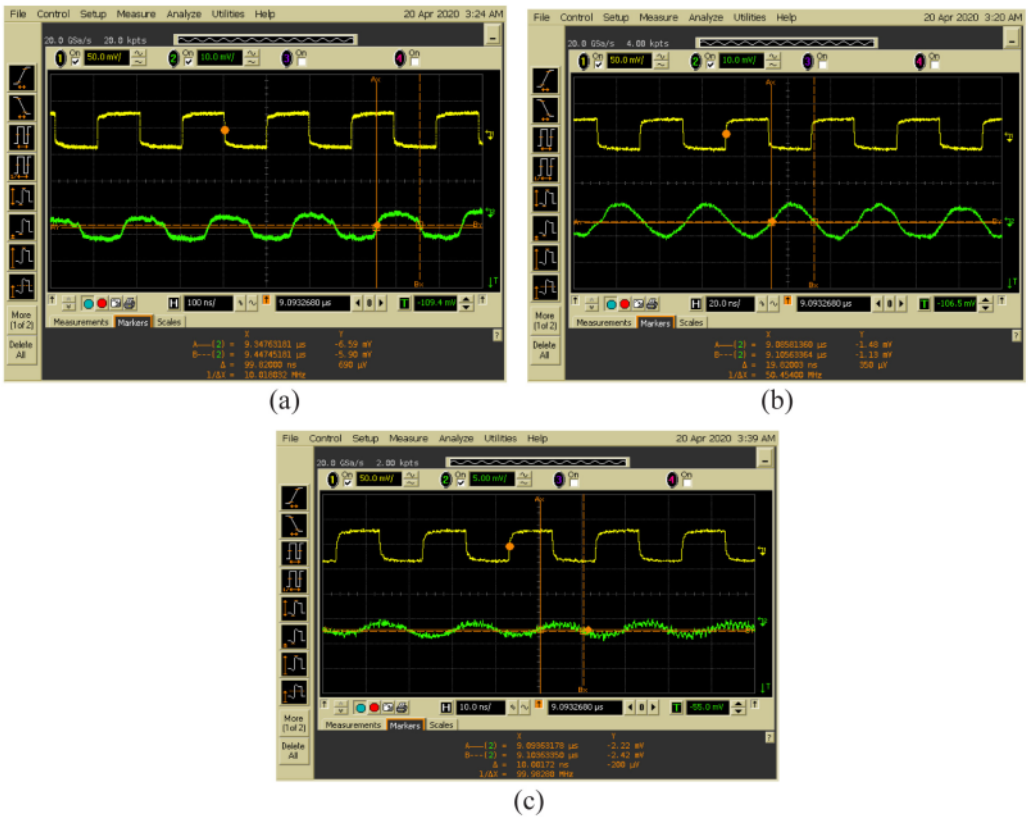

Fig. 16. Waveform of λ_2 originating from the *Rc* in the CEH circuit under the bit rates of (a) 10 Mbps, (b) 50 Mbps, and (c) 100 Mbps.

Table 4
CEH parameters under different signal frequencies for λ_2.

CEH parameters	Frequency		
	100 kHz	10 MHz	15 MHz
DC current	0.97 mA	0.98 mA	0.99 mA
DC voltage	0.58 mV	0.59 mV	0.60 mV
AC voltage	83.30 mV_{pp}	72.90 mV_{pp}	72.40 mV_{pp}

Table 5
CEH parameters under different bit rates for λ_2.

CEH parameters	Bit rate		
	10 Mbps	50 Mbps	100 Mbps
DC current	0.98 mA	0.97 mA	0.97 mA
DC voltage	0.59 mV	0.58 mV	0.58 mV

4. Conclusions

A fiber-based resonant beam system was applied to enable simultaneous information and power transmission through free space. Two pairs of FBGs with different wavelengths (λ_1 and λ_2) were used to realize optical resonance and data transmission for multiuser applications. An EOM was used to modulate the optical signals for broadcast information transmission and simultaneously present them in the fiber loop. After the resonance effect had been achieved, some of the optical signals were transmitted to the PIN PD for AC–DC signal separation for power and information harvesting; the other optical signals were fed back to the fiber loop to complete the resonance effect.

The experiments proved that the power attenuation in the fiber loop was relatively small. More significant power attenuation occurred after the signals passed through free space, where the power dropped by approximately 5 dBm. The power attenuation in free space influenced the photocurrent generated by the PIN PD, resulting in the generation of small DC and AC voltages in the harvesting subsystem. Under the multiuser scheme, the result was approximately 0.55 dBm lower than that under the single-user scheme.

Although power attenuation in free space is a vital consideration that warrants optimization in future research, the experimental results obtained in this study proved that it is possible to use an all-fiber resonant beam system for simultaneous OWIPT.

Declaration of competing interest

The authors declare that they have no known competing financial interests or personal relationships that could have appeared to influence the work reported in this paper.

Acknowledgment

This work was supported by the Ministry of Science and Technology, Taiwan, under Grants MOST 108-2221-E-150-041 and MOST 107-2218-E-150-008-MY2.

References

[1] A. Morgado, K.M.S. Huq, S. Mumtaz, J. Rodriguez, A survey of 5G technologies: regulatory, standardization and industrial perspectives, Digit. Commun. Netw. 4 (2018) 87–97.

[2] V.W.S. Chan, Free-space optical communications, J. Lightwave Technol. 24 (2006) 4750–4762.
[3] A. Kurs, et al., Wireless power transfer via strongly coupled magnetic resonances, Science 317 (5834) (2007) 83–86.
[4] P. Sample, D.T. Meyer, J.R. Smith, Analysis, experimental results, and range adaptation of magnetically coupled resonators for wireless power transfer, IEEE Trans. Ind. Electron. 58 (2) (2011) 544–554.
[5] M. Xiong, Q. Liu, M. Liu, X. Wang, H. Deng, Resonant beam communications with photovoltaic receiver for optical data and power transfer, IEEE Trans. Commun. 68 (5) (2020) 3033–3041.
[6] D. Killinger, Free space optics for laser communication through the air, Opt. Photonics News 13 (2002) 36–42.
[7] K. Sung-Man, R. Dong-Hun, Experimental demonstration of optical wireless power transfer with a DC-to-DC transfer efficiency of 12.1%, Opt. Eng., Bellingham 57 (8) (2018) 086108.
[8] W. Zhou, K. Jin, Efficiency evaluation of laser diode in different driving modes for wireless power transmission, IEEE Trans. Power Electron. 30 (2015) 6237–6244.
[9] W.J. Wang, C. Huang, A coupled model on energy conversion in laser power beaming, J. Power Sources 393 (2018) 211–216.
[10] H.S. Dhadwal, J. Rastegar, P. Kwok, Wireless energy and data transfer to munitions using high power laser diodes, in: Proc. SPIE 10195, Unmanned Systems Technology XIX, 2017, p. 1019513.
[11] C.D. Santi, M. Meneghini, A. Caria, E. Dogmus, M. Zegaoui, F. Medjdoub, B. Kalinic, T. Cesca, G. Meneghesso, E. Zanoni, GaN-based laser wireless power transfer system, Materials 11 (1) (2018) 153.
[12] Z. Yuhuan, T. Miyamoto, 200 mW-class LED-based optical wireless power transmission for compact IoT, Japan. J. Appl. Phys. 58 (2019) SJJC04.
[13] J. Mukherjee, et al., Efficiency limits of laser power converters for optical power transfer applications, J. Phys. D: Appl. Phys. 46 (2013) 264006.
[14] Q. Liu, et al., Charging unplugged: Will distributed laser charging for mobile wireless power transfer work? IEEE Veh. Technol. Mag. 11 (4) (2016) 36–45.
[15] Q. Zhang, et al., Distributed laser charging: A wireless power transfer approach, IEEE Internet Things J. 5 (5) (2018) 3853–3864.
[16] H. Tran, G. Kaddoum, C. Abou-Rjeily, Collaborative RF and lightwave power transfer for next-generation wireless networks, IEEE Commun. Mag. 58 (2) (2020) 27–33.
[17] G.F. Pan, P.D. Diamantoulakis, Z. Ma, Z.G. Ding, G.K. Karagiannidis, Simultaneous lightwave information and power transfer: Policies, techniques and future directions, IEEE Access 7 (2019) 28250–28257.
[18] J. Lim, T.S. Khwaja, J.Y. Ha, Wireless optical power transfer system by spatial wavelength division and distributed laser cavity resonance, Opt. Express 27 (2019) A924–A935.
[19] Z. Wang, et al., On the design of a solar-panel receiver for optical wireless communications with simultaneous energy harvesting, IEEE J. Sel. Areas Commun. 33 (8) (2015) 1612–1623.

EDDY WIJANTO-FILE 8

ORIGINALITY REPORT

6%	4%	5%	2%
SIMILARITY INDEX	INTERNET SOURCES	PUBLICATIONS	STUDENT PAPERS

PRIMARY SOURCES

1	rimsi.imsi.bg.ac.rs Internet Source	1%
2	Panagiotis D. Diamantoulakis, George K. Karagiannidis, Zhiguo Ding. "Simultaneous Lightwave Information and Power Transfer (SLIPT)", IEEE Transactions on Green Communications and Networking, 2018 Publication	1%
3	jati-kuantansingingi-kuansing-riau.blogspot.com Internet Source	1%
4	www.semanticscholar.org Internet Source	1%
5	Qingqing Zhang, Wen Fang, Qingwen Liu, Jun Wu, Pengfei Xia, Liuqing Yang. "Distributed Laser Charging: A Wireless Power Transfer Approach", IEEE Internet of Things Journal, 2018 Publication	1%
6	Submitted to Oregon State University Student Paper	<1%

7	Yin-Yann Chen, Chen-Yang Cheng, Jia-Ying Li. "Resource-constrained assembly line balancing problems with multi-manned workstations", Journal of Manufacturing Systems, 2018 Publication	<1 %
8	Submitted to King Abdullah University of Science and Technology (KAUST) Student Paper	<1 %
9	M.R. Marcin. "Digital Receiver Phase Meter for LISA", IEEE Transactions on Instrumentation and Measurement, 2005 Publication	<1 %
10	Mohammad Furqan Ali, Dushantha Nalin K. Jayakody, Yonghui Li. "Recent Trends in Underwater Visible Light Communication (UVLC) Systems", IEEE Access, 2022 Publication	<1 %
11	downloads.hindawi.com Internet Source	<1 %
12	"6G Mobile Wireless Networks", Springer Science and Business Media LLC, 2021 Publication	<1 %

Exclude quotes	On	Exclude matches	< 15 words
Exclude bibliography	On		